Effects of the phase of a laser field on autoionization

Takashi Nakajima and P. Lambropoulos
Max-Planck-Institut für Quantenoptik, D-85748, Garching, Germany;
Institute of Electronic Structure and Laser, FORTH, and Department of Physics, University of Crete, P.O. Box 1527, Heraklion 711 10, Crete, Greece;
Department of Physics, University of Southern California, Los Angeles, California 90089-0484
(Received 28 December 1993)

We present a formal theory and detailed calculations for phase-dependent laser-atom interactions involving autoionizing states. First, through simple models, we demonstrate that the simultaneous one- and three-photon excitation of one or two neighboring autoionizing states can exhibit profound changes of the line shape, as the relative phase of the two fields is varied from 0 to π. Through a proper choice of the field intensities and the phase, we obtain analytical results showing that one can cancel the transition to the discrete or the continuum part of the wave function, thereby leading to a flat or a completely symmetric line shape, respectively. At higher intensities, additional effects come into play, providing additional coupling between the discrete and continuum parts, which also exhibits a phase dependence. Finally, our theory is applied to a much more complex situation in Xe, involving many channels, not amenable to simple analytical expressions, but exhibiting nevertheless equally profound effects, including a modification of the branching ratio of two different products. The theory, which is here developed for atomic autoionization, is in fact fairly general and should pertain to related problems in any system involving discrete states embedded in continua.

PACS number(s): 42.50.Hz, 42.65.Ky, 32.80.Rm

I. INTRODUCTION

In a recent paper [1], we presented our main results on the effect of the phase of the field on the excitation of an autoionizing resonance. Specifically, we have developed a theory and have performed related calculations which demonstrate that, under the combined excitation by a single- and a three-photon transition, mediated by two separate fields whose relative phase is controllable, the autoionization line shape undergoes profound changes as the phase is varied from 0 to π. It is the purpose of this paper to present a complete account of the work including a detailed exposition of the theory, as well as a more extensive discussion of the results and their implications.

The subject matter of this work belongs to the general area of what is referred to as the "coherent control" of photoionization in atoms [1–8] and molecules [9–19], which has been receiving considerable attention during the last five years or so. The basic idea is appealing and potentially of broad impact. If one can alter the strength of a transition for selected channels, one can in principle control the branching ratio of products with obvious implications for chemistry [9–17]. Various methods for achieving control of branching ratios have been proposed; e.g., introducing a pulse delay between ultrafast pulses [12–15], exploiting the polarization of the laser fields [16], and of course manipulating the phase of laser fields [9–11,17–19]. Achieving this through the phase of the field [1–11,17–19] has a certain appeal of simplicity, although the technical requirements for its experimental implementation are far from trivial. In addition to its possible impact on photochemistry, the idea certainly offers a novel way of exploring atomic structure, especially above the first ionization threshold. The possibility of turning off channels into the continuum raises the prospect of perhaps stabilizing (at least partially) an excited state with interesting consequences on nonlinear optical processes.

Our choice of focusing this series of studies on autoionizing states stems from the fact that they represent prototypes of channel coupling which also involve continua. Most of the discussion of phase control has centered on transitions between bound states. It was not evident that the scheme would work equally well in transitions into a continuum. We have shown in separate work [4] that phase control can indeed be extended to transitions directly into a structureless continuum. An autoionizing state, however, represents a more complex situation in that it involves a continuum which acquires structure due to intra-atomic interactions. In our work as discussed herein, we have explored these questions beginning with simple models that encapsulate the essential physics and then proceed to rather complicated situations involving several coupled channels. As discussed in detail later on, the basic effects found in the simple models persist in the more complex situations. Although our specific study refers to autoionization in an atom, the context is more general and would be equally applicable to any situation involving discrete states embedded in continua, independent of whether these continua represent ionization or dissociation.

Most of our discussion is centered around situations with relatively moderate intensities so that the atomic structure and channels are not distorted by the field and transition amplitudes in perturbation theory are applicable. In general, intensity effects [20,21] may manifest

1050-2947/94/50(1)/595(16)/$06.00

themselves at higher intensities. We devote a small part of our discussion to such effects, which may or may not be of interest in this context. That remains to be seen.

The following is the outline of this paper. Section II is devoted to the formulation for the atomic system we study. We first derive the time-dependent density-matrix equations for a single autoionizing state coupled to a bound state by both a single- and a three-photon process, whose relative phase of the fields is well defined. Then, a time-independent single-rate equation is derived from the density-matrix equations to obtain a simple physical picture. We further investigate the intensity effect mentioned above. As a generalization of our formalism, a set of density-matrix equations and a single-rate equation are obtained for two autoionizing states coupled to a bound state by two fields as before. Results are presented in Sec. III. As a demonstration that phase effects may be observed in a much more complicated system, we present in Sec. IV several MQDT (multichannel quantum defect theory, [25,26]) calculations on the Xe atom. Autoionization spectra and photoelectron angular distributions are shown for various laser intensities and relative phase values. A summary is given in Sec. V.

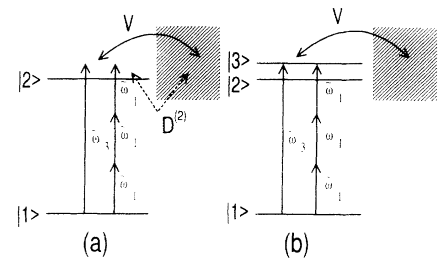

FIG. 1. Schemes studied in this paper. The shaded area is the atomic continuum. One bound state $|1\rangle$ and one (two) autoionizing state(s) $|2\rangle$ (and $|3\rangle$) are coupled by two fields with frequencies $\tilde{\omega}_1$ and $\tilde{\omega}_3=3\tilde{\omega}_1$ and the relative phase ϕ. (a) Single autoionizing state. (b) Two autoionizing states. The dashed line in (a), denoted as $D^{(2)}$, is the two-photon coupling between $|2\rangle$ and continuum state (shaded area). As the field intensity with frequency $\tilde{\omega}_1$ increases, the amplitude of this radiative coupling $D^{(2)}$ increases and may become comparable to the intra-atomic configuration interaction V, and autoionization spectra may be significantly modified. This effect will be examined in Sec. II A 3. For simplicity, we shall not consider the intensity effect for (b).

II. SYSTEM DESCRIPTION

A. Single autoionizing state

1. *Density-matrix equations for a single autoionizing state*

We begin with the formulation of our system by considering one bound state $|1\rangle$ (usually the ground state) and one autoionizing state (AIS) $|2\rangle$ with opposite parity. The energies of these states are denoted by $\hbar\omega_j$ ($j=1$ or 2). We are, in particular, interested in the case where $|1\rangle$ is coupled to the vicinity of $|2\rangle$ by the simultaneous action of radiation at frequency $\tilde{\omega}_1$ and its third harmonic $\tilde{\omega}_3=3\tilde{\omega}_1$ [Fig. 1(a)]. The intensities of these fields are denoted by I_1 and I_3, respectively. An important ingredient of our problem is the relative phase ϕ of the amplitudes of the fields ε_1 and ε_3, which we assume to be controllable and whose effect on the photoabsorption and its products is the central theme of this paper. Under these assumptions, the total electric field interacting with the atom can be written as

$$E(t)=(\varepsilon_1 e^{i\tilde{\omega}_1 t}+\varepsilon_3 e^{i(\tilde{\omega}_3 t+\phi)})+\text{c.c.} , \tag{1}$$

which is assumed to be linearly polarized along the z axis. A generalization of the standard procedure [21–23] (whose steps are shown in Appendix A) leads to the following set of density-matrix equations:

$$\frac{\partial}{\partial t}\sigma_{11}=-\gamma\sigma_{11}+2\,\mathrm{Im}\left\{\left[\Omega_2^{(3)}\left[1-\frac{i}{q_2^{(3)}}\right]+e^{i\phi}\Omega_2\left[1-\frac{i}{q_2}\right]\right]\sigma_{21}\right\} , \tag{2}$$

$$\frac{\partial}{\partial t}\sigma_{22}=-\Gamma_2\sigma_{22}-2\,\mathrm{Im}\left\{\left[\Omega_2^{(3)}\left[1+\frac{i}{q_2^{(3)}}\right]+e^{i\phi}\Omega_2\left[1+\frac{i}{q_2}\right]\right]\sigma_{21}\right\} , \tag{3}$$

$$\begin{aligned}\left[\frac{\partial}{\partial t}-i\delta_2+\tfrac{1}{2}(\gamma+\Gamma_2)\right]\sigma_{21}=&-i\left[\Omega_2^{(3)}\left[1-\frac{i}{q_2^{(3)}}\right]+e^{-i\phi}\Omega_2\left[1-\frac{i}{q_2}\right]\right]\sigma_{11}\\&+i\left[\Omega_2^{(3)}\left[1+\frac{i}{q_2^{(3)}}\right]+e^{-i\phi}\Omega_2\left[1+\frac{i}{q_2}\right]\right]\sigma_{22} ,\end{aligned} \tag{4}$$

where γ is the effective ionization width directly into the continuum, given by

$$\gamma=2\left|\frac{\Omega_2^{(3)}}{q_2^{(3)}\sqrt{\Gamma_2/2}}+e^{i\phi}\frac{\Omega_2}{q_2\sqrt{\Gamma_2/2}}\right|^2+\gamma_{\text{incoherent}}^{(3)}$$
$$\equiv|\sqrt{\gamma^{(3)}}+e^{i\phi}\sqrt{\gamma^{(1)}}|^2+\gamma_{\text{incoherent}}^{(3)}\ .$$

The quantities $\gamma^{(1)}$, $\gamma^{(3)}$, and $\gamma_{\text{incoherent}}$, which describe, respectively, the direct ionization width into the continuum by a single photon $\bar{\omega}_3$, or by three photons $\bar{\omega}_1$, and the three-photon ionization width into the continuum, which is accessible only through the three-photon process (incoherent contribution to the ionization) due to the dipole selection rule, have also been introduced here. $\Omega_2^{(3)}$ and Ω_2 are three- and single-photon Rabi frequencies between states $|2\rangle$ and $|1\rangle$, respectively, and Γ_2 is the autoionization width of state $|2\rangle$. $\delta_2\equiv 3\bar{\omega}_1-(\bar{\omega}_2-\bar{\omega}_1)$ (note that $\bar{\omega}_1$ and $\bar{\omega}_2$ are perturbed energy levels of states $|1\rangle$ and $|2\rangle$, respectively) gives the detuning and $q_2^{(3)}$, q_2 are three- and one-photon asymmetry parameters of state $|2\rangle$. It should be stressed at this point that an AIS is modelled here as a discrete state embedded in a *single* continuum. In reality, the situation is usually more complicated than that, and one must perform sophisticated and elaborate atomic structure calculations for real atoms, in order to obtain the atomic parameters we have defined above. Nevertheless, we begin our discussion with this simple model in order to understand the essence of phase effects.

2. Single-rate approximation for a single autoionizing state

To analyze the system we have described above, the time-dependent density-matrix equations must in principle be solved. However, we first consider the case in weak electromagnetic fields. By weak, we mean $\Gamma_2\gg\gamma^{(1)},\gamma^{(3)},\Omega_2,\Omega_2^{(3)}$. In this limit, the photoionization line shape can be obtained in terms of a transition rate (Fermi's golden rule) without any time-dependent calculations. From the set of density-matrix equations for a single AIS [Eqs. (2)–(4)], the single-ionization rate is obtained by assuming weak transitions out of $|1\rangle$, which implies $\sigma_{11}(t)\sim 1$, $\sigma_{22}(t)\sim 0$, and $\dot{\sigma}_{21}(t)=0$. Then we can solve for σ_{21}, obtaining

$$\sigma_{21}=\frac{-i}{i\delta_2+(\gamma+\Gamma_2)/2}\left[\Omega_2^{(3)}\left[1-\frac{i}{q_2^{(3)}}\right]+e^{-i\phi}\Omega_2\left[1-\frac{i}{q_2}\right]\right]\ . \tag{5}$$

Substituting this into Eq. (2) and defining $\epsilon_2\equiv\delta_2/(\Gamma_2/2)$, which is a dimensionless detuning in units of the autoionization halfwidth, we obtain

$$\sigma_{11}=-\gamma-\frac{1}{1+\epsilon^2}\left\{\left|\frac{\Omega_2^{(3)}}{q_2^{(3)}\sqrt{\Gamma_2/2}}(q_2^{(3)}+\epsilon)+e^{i\phi}\frac{\Omega_2}{q_2\sqrt{\Gamma_2/2}}(q_2+\epsilon)\right|^2-(\epsilon^2+1)\left[\frac{(\Omega_2^{(3)})^2}{(q_2^{(3)})^2\Gamma_2/2}+\frac{(\Omega_2)^2}{(q_2)^2\Gamma_2/2}+2\cos\phi\frac{\Omega_2^{(3)}\Omega_2}{q_2^{(3)}q_2\Gamma_2/2}\right]\right\}\ . \tag{6}$$

Noting that

$$\gamma=2\left[\frac{(\Omega_2^{(3)})^2}{(q_2^{(3)})^2\Gamma_2/2}+\frac{(\Omega_2)^2}{(q_2)^2\Gamma_2/2}+2\cos\phi\frac{\Omega_2^{(3)}\Omega_2}{q_2^{(3)}q_2\Gamma_2/2}\right]\ , \tag{7}$$

the photoionization rate P is written as

$$P=-\dot{\sigma}_{11}\propto\frac{1}{\epsilon^2+1}\left|\frac{\Omega_2^{(3)}}{q_2^{(3)}\sqrt{\Gamma_2/2}}(q_2^{(3)}+\epsilon)+e^{i\phi}\frac{\Omega_2}{q_2\sqrt{\Gamma_2/2}}(q_2+\epsilon)\right|^2\ . \tag{8}$$

This is nothing but the coherent superposition of the transition amplitudes [24] due to the two fields between the same initial and final states. This form is to be expected, in the single-rate limit, since the density-matrix equations are additive with respect to the two fields.

3. Intensity effect within a single-rate approximation

We proceed now one step beyond the lowest order single-rate approximation by considering the lowest order correction due to the intensity. It had been pointed out some time ago [20] that in a three-photon coupling of an AIS with a bound state, the first intensity effect to be expected is represented by a two-photon (Raman-type) coupling between the discrete state and the continuum to which it is coupled by configuration interaction [see Fig. 1(a)]. It would be expected to influence the transition process significantly when the intensity is such that this two-photon process (whose amplitude is proportional to the intensity I) becomes comparable to the configuration-interaction matrix element that determines the autoionization width [20]. Given that the three-photon transition amplitude to the autoionizing state is proportional to the laser intensity $I^{3/2}$, there should in general be an intensity range for which this will be the dominant intensity effect, before other intensity effects such as the saturation of the three-photon transition set in. The net effect of this correction due to the intensity is to modify (through the addition of intensity-dependent terms) the Rabi frequency and the q parameters and to introduce an effective configuration interaction $\tilde{V}$, which involves the intensity-dependent two-photon transition mentioned above. In this paper, all quantities with ("$\sim$") indicate that they are intensity dependent. From now on, we use the notation $\mathrm{P}\sum_c$ to represent the principal-value integration over all possible (both bound and continuum) states $|c\rangle$. With the explicit terms which depend on the laser intensities I_1 and I_3 with frequencies $\tilde{\omega}_1$ and $\tilde{\omega}_3$, respectively, the intensity-dependent $\tilde{q}$ parameters and Rabi frequencies $\tilde{\Omega}$ may be written as

$$\tilde{\Omega}_2^{(3)}=\hbar^{-1}\mu_{12}^{(3)}\varepsilon_1^3+\mathrm{P}\sum_c \frac{\mu_{1c}^{(3)}\varepsilon_1^3\tilde{V}_{c2}}{\hbar^2(3\tilde{\omega}_1-\omega_{c1})}$$

$$=(A+\alpha^{(5)}I_1)I_1^{3/2}\ , \tag{9}$$

$$\tilde{q}_2^{(3)}=\frac{\tilde{\Omega}_2^{(3)}}{\pi\hbar^{-2}(\mu_{1c}^{(3)}\varepsilon_1^3\tilde{V}_{c2})_{\omega_c=\omega_1+3\tilde{\omega}_1}}$$

$$=\frac{(A+\alpha^{(5)}I_1)q_2^{(3)}}{A+q_2^{(3)}\beta^{(5)}I_1}\ , \tag{10}$$

$$\tilde{\Omega}_2=\hbar^{-1}\mu_{12}\varepsilon_3+\mathrm{P}\sum_c \frac{\mu_{1c}\varepsilon_3\tilde{V}_{c2}}{\hbar^2(3\tilde{\omega}_1-\omega_{c1})}$$

$$=(B+\alpha^{(3)}I_1)I_3^{1/2}\ , \tag{11}$$

$$\tilde{q}_2=\frac{\tilde{\Omega}_2}{\pi\hbar^{-2}(\mu_{1c}\varepsilon_3\tilde{V}_{c2})_{\omega_c=\omega_1+3\tilde{\omega}_1}}=\frac{(B+\alpha^{(3)}I_1)q_2}{B+q_2\beta^{(3)}I_1}\ , \tag{12}$$

$$\tilde{\varepsilon}=\frac{\delta_2}{\tilde{\Gamma}_2/2}\ , \tag{13}$$

with

$$\begin{aligned}
&\tilde{V}_{c2}\equiv V_{c2}+\mu_{c2}^{(2)}(\varepsilon_1)^2\ ,\\
&\tilde{\Gamma}_2\equiv 2\pi|\tilde{V}_{c2}|^2_{\omega_c=\omega_1+3\tilde{\omega}_1}\ ,\\
&\tilde{\Omega}_2^{(3)}\equiv\frac{\mu_{12}^{(3)}(\varepsilon_1)^3}{\hbar}+\mathrm{P}\sum_c\frac{\mu_{1c}^{(3)}(\varepsilon_1)^3V_{c2}}{\hbar^2(3\tilde{\omega}_1-\omega_{c1})}\equiv AI_1^{3/2}\ ,\\
&\alpha^{(5)}\equiv\mathrm{P}\sum_c\frac{\mu_{1c}^{(3)}\mu_{c2}^{(2)}}{\hbar^2(3\tilde{\omega}_1-\omega_{c1})}\ ,\\
&\beta^{(5)}\equiv\pi\hbar^{-2}(\mu_{1c}^{(3)}\mu_{c2}^{(2)})_{\omega_c=\omega_1+3\tilde{\omega}_1}\ ,\\
&\tilde{\Omega}_2\equiv\frac{\mu_{12}\varepsilon_3}{\hbar}+\mathrm{P}\sum_c\frac{\mu_{1c}\varepsilon_3V_{c2}}{\hbar^2(3\tilde{\omega}_1-\omega_{c1})}\equiv BI_3^{1/2}\ ,\\
&\alpha^{(3)}\equiv\mathrm{P}\sum_c\frac{\mu_{1c}\mu_{c2}^{(2)}}{\hbar^2(3\tilde{\omega}_1-\omega_{c1})}\ ,\\
&\beta^{(3)}\equiv\pi\hbar^{-2}(\mu_{1c}\mu_{c2}^{(2)})_{\omega_c=\omega_1+3\tilde{\omega}_1}\ .
\end{aligned} \tag{14}$$

In the above equations, μ_{ij} and $\mu_{ij}^{(n)}$ indicate the single- and effective n-photon electric dipole matrix elements between states $|i\rangle$ and $|j\rangle$. In Sec. III A 3, we will plot the graphs as a function of this dimensionless but intensity dependent $\tilde{\varepsilon}$, normalized by the intensity-dependent autoionization width $\tilde{\Gamma}_2$. It may be worth stressing that $\tilde{\Omega}_2$, $\tilde{q}_2$, $\tilde{\Omega}_2^{(3)}$, and $\tilde{q}_2^{(3)}$ are intensity dependent through the effective configuration interaction $\tilde{V}_{c2}$ due to the photon $\tilde{\omega}_1$. Introducing the parameters defined above, the photoionization rate P [Eq. (8)] is rewritten as

$$P\propto\frac{1}{\tilde{\varepsilon}^2+1}\left|\frac{\tilde{\Omega}_2^{(3)}}{\tilde{q}_2^{(3)}}(\tilde{q}_2^{(3)}+\tilde{\varepsilon})+e^{i\phi}\frac{\tilde{\Omega}_2}{\tilde{q}_2}(\tilde{q}_2+\tilde{\varepsilon})\right|^2\ . \tag{15}$$

We further rewrite this expression in terms of the following intensity-independent parameters:

$$\alpha'\equiv\frac{\alpha^{(5)}}{A}\ ,\quad \beta'\equiv\frac{\beta^{(5)}}{A}\ ,\quad \alpha\equiv\frac{\alpha^{(3)}}{B}\ ,\quad \beta\equiv\frac{\beta^{(3)}}{B}\ , \tag{16}$$

in the form

$$P\propto\frac{1}{(1+q_2^{(3)}\beta'I_1)^2\epsilon^2+1}\times\left|\Omega_2^{(3)}\left[(1+\alpha'I_1)+\frac{\epsilon}{q_2^{(3)}}(1+q_2^{(3)}\beta'I_1)^3\right]+e^{i\phi}\Omega_2\left[(1+\alpha I_1)+\frac{\epsilon}{q_2}(1+q_2\beta I_1)^3\right]\right|^2\ , \tag{17}$$

which exhibits explicitly the intensity-dependent parts. Clearly, by setting $I_1\rightarrow 0$, one immediately obtains Eq. (8). Assuming a single continuum, $\tilde{\varepsilon}$ and ε are related with $\tilde{\varepsilon}=(q_2\tilde{\Omega}_2/\tilde{q}_2\Omega_2)^2\epsilon=(q_2^{(3)}\tilde{\Omega}_2^{(3)}/\tilde{q}_2^{(3)}\Omega_2^{(3)})^2\epsilon$. Alternatively, $\tilde{\varepsilon}=(1+q_2\beta I_1)^2\epsilon=(1+q_2^{(3)}\beta'I_1)^2\epsilon$. This equation also imposes a restriction between β and β', namely $q_2\beta=q_2^{(3)}\beta'$.

We are interested in the change of the photoionization rate P as a function of the intensity I_1. If I_1 is increased with "fixed" I_3, the phase-dependent interference will of course eventually decrease, since the three-photon transition will become dominant over the single-photon transition. Hence it should be understood that I_3 is also assumed to be increased as I_1 is increased, so that $\Omega_2^{(3)}/\Omega_2=\text{const}$. In the numerical results which will be shown in Sec. III, intensity effects are not taken into account unless otherwise mentioned explicitly.

B. Two autoionizing states

1. Density-matrix equations for two autoionizing states

The extension of our formalism to the case which involves two AIS's of the same parity connected to a common bound state by two laser fields [Fig. 1(b)] is straightforward. The set of density-matrix equations can be expressed as

$$\frac{\partial}{\partial t}\sigma_{11}=-\gamma\sigma_{11}+2\sum_{j=2,3}\mathrm{Im}\left\{\left[\Omega_j^{(3)}\left[1-\frac{i}{q_j^{(3)}}\right]+e^{i\phi}\Omega_j\left[1-\frac{i}{q_j}\right]\right]\sigma_{j1}\right\}, \tag{18}$$

$$\frac{\partial}{\partial t}\sigma_{jj}=-\Gamma_j\sigma_{jj}-2\,\mathrm{Im}\left\{\left[\Omega_j^{(3)}\left[1+\frac{i}{q_j^{(3)}}\right]+e^{i\phi}\Omega_j\left[1+\frac{i}{q_j}\right]\right]\sigma_{j1}\right\}\quad (j=2,3), \tag{19}$$

$$\begin{aligned}\left[\frac{\partial}{\partial t}-i\delta_j+\tfrac{1}{2}(\gamma+\Gamma_j)\right]\sigma_{j1}=&-i\left[\Omega_j^{(3)}\left[1-\frac{i}{q_j^{(3)}}\right]+e^{-i\phi}\Omega_j\left[1-\frac{i}{q_j}\right]\right]\sigma_{11}\\&+i\left[\Omega_j^{(3)}\left[1+\frac{i}{q_j^{(3)}}\right]+e^{-i\phi}\Omega_j\left[1+\frac{i}{q_j}\right]\right]\sigma_{jj}\\&+i\left[\Omega_k^{(3)}\left[1+\frac{i}{q_k^{(3)}}\right]+e^{-i\phi}\Omega_k\left[1-\frac{i}{q_k}\right]\right]\sigma_{jk}\quad (j,k=2,3 \text{ and } j\neq k),\end{aligned} \tag{20}$$

$$\begin{aligned}\left[\frac{\partial}{\partial t}-i(\delta_3-\delta_2)+\tfrac{1}{2}(\Gamma_2+\Gamma_3)\right]\sigma_{32}=&-i\left[\Omega_3^{(3)}\left[1-\frac{i}{q_3^{(3)}}\right]+e^{-i\phi}\Omega_3\left[1-\frac{i}{q_3}\right]\right]\sigma_{12}\\&+i\left[\Omega_2^{(3)}\left[1+\frac{i}{q_2^{(3)}}\right]+e^{i\phi}\Omega_2\left[1+\frac{i}{q_2}\right]\right]\sigma_{31}.\end{aligned} \tag{21}$$

As in Sec. II A 1, $\Omega_j^{(3)}$ and Ω_j $(j=2,3)$ are three- and single-photon Rabi frequencies between state $|j\rangle$ and $|1\rangle$, respectively, and Γ_j $(j=2,3)$ is the autoionization width of state $|j\rangle$. The detuning is defined as $\delta_j\equiv 3\bar{\omega}_1-(\bar{\omega}_j-\bar{\omega}_1)$ (note that $\bar{\omega}_1$ and $\bar{\omega}_j$ are perturbed energy levels of states $|1\rangle$ and $|j\rangle$, respectively) and $q_j^{(3)}$, q_j $(j=2,3)$ are three- and one-photon asymmetry parameters of the state $|j\rangle$. We are assuming a single continuum for both AIS's $|2\rangle$ and $|3\rangle$. One should notice that the direct ionization widths $\gamma^{(1)}$ and $\gamma^{(3)}$ are then the same for both $|2\rangle$ and $|3\rangle$. Noting that both $\gamma^{(1)}$ and $\gamma^{(3)}$ should be describable in terms of parameters for $|2\rangle$ and $|3\rangle$ equivalently, we have

$$\gamma^{(1)}=\frac{4(\Omega_2)^2}{q_2^2\Gamma_2}=\frac{4(\Omega_3)^2}{q_3^2\Gamma_3} \tag{22}$$

and

$$\gamma^{(3)}=\frac{4(\Omega_2^{(3)})^2}{(q_2^{(3)})^2\Gamma_2}=\frac{4(\Omega_3^{(3)})^2}{(q_3^{(3)})^2\Gamma_3}. \tag{23}$$

This restriction, however, will be lifted if incoherent channels exists.

2. Single-rate approximation for two autoionizing states

A single-rate approximation can be made for two AIS's as well, by following the procedure described in Sec. II A 2. For a single laser field, the photoionization rate P is written as

$$P\propto\frac{(q_2\epsilon_3+q_3\epsilon_2+\epsilon_2\epsilon_3)^2}{(\epsilon_2\epsilon_3)^2+(\epsilon_2+\epsilon_3)^2}, \tag{24}$$

where q_i and ϵ_i $(i=2,3)$ are the q value and the dimensionless detuning from the states $|2\rangle$ and $|3\rangle$ in units of Γ_2 and Γ_3, respectively. A detailed derivation of this rate equation is given in Appendix B. We now turn on two sources with frequencies $\tilde{\omega}_1$ and $\tilde{\omega}_3$, whose phase difference is defined as ϕ. We can immediately write down the photoionization rate for two AIS's, which reads

$$\begin{aligned}P&\propto\frac{1}{(\epsilon_2\epsilon_3)^2+(\epsilon_2+\epsilon_3)^2}\left|\frac{\Omega_2^{(3)}}{q_2^{(3)}\sqrt{\Gamma_2/2}}(q_2^{(3)}\epsilon_3+q_3^{(3)}\epsilon_2+\epsilon_2\epsilon_3)+e^{i\phi}\frac{\Omega_2}{q_2\sqrt{\Gamma_2/2}}(q_2\epsilon_3+q_3\epsilon_2+\epsilon_2\epsilon_3)\right|^2\\&\propto\frac{1}{(\epsilon_2\epsilon_3)^2+(\epsilon_2+\epsilon_3)^2}\left|\Omega_2^{(3)}\left[\epsilon_3+\frac{q_3^{(3)}}{q_2^{(3)}}\epsilon_2+\frac{\epsilon_2\epsilon_3}{q_2^{(3)}}\right]+e^{i\phi}\Omega_2\left[\epsilon_3+\frac{q_3}{q_2}\epsilon_2+\frac{\epsilon_2\epsilon_3}{q_2}\right]\right|^2.\end{aligned} \tag{25}$$

Alternatively,

$$\begin{aligned}P&\propto\frac{1}{(\epsilon_2\epsilon_3)^2+(\epsilon_2+\epsilon_3)^2}\left|\frac{\Omega_2^{(3)}}{q_2^{(3)}\sqrt{\Gamma_2/2}}(q_2^{(3)}\epsilon_3+q_3^{(3)}\epsilon_2+\epsilon_2\epsilon_3)+e^{i\phi}\frac{\Omega_2}{q_2\sqrt{\Gamma_2/2}}(q_2\epsilon_3+q_3\epsilon_2+\epsilon_2\epsilon_3)\right|^2\\&\propto\frac{1}{(\epsilon_2\epsilon_3)^2+(\epsilon_2+\epsilon_3)^2}\left|\Omega_3^{(3)}\left[\frac{q_2^{(3)}}{q_3^{(3)}}\epsilon_3+\epsilon_2+\frac{\epsilon_2\epsilon_3}{q_3^{(3)}}\right]+e^{i\phi}\Omega_3\left[\frac{q_2}{q_3}\epsilon_3+\epsilon_2+\frac{\epsilon_2\epsilon_3}{q_3}\right]\right|^2.\end{aligned} \tag{26}$$

This is the consequence of our assumption that both autoionizing states are coupled to the same single continuum state. If $|\epsilon_3| \gg |\epsilon_2|$, this equation reduces to the expression for the single AIS case, as it should be. Obviously, from the above expressions, it is possible to suppress the photoionization from one of the two AIS by choosing the proper relative phase and laser intensities, depending on the q values. Without any fundamental difficulty, we could explore the equations which include intensity effects for two AIS's, as in Sec. II A 3 for a single AIS. We shall not consider this case here, however, since our purpose in this paper is to demonstrate the important features for a simple system.

III. RESULTS AND DISCUSSION

A. Single autoionizing state

1. Weak-field limit

As shown in the previous sections, the photoionization rate P, under the presence of two laser fields which couple the initial and final states by single- and three-photon transitions, is written as a coherent superposition of the two photoionization rates. It follows that we can control the ionization rate by manipulating the relative phase of the two laser fields without changing the laser intensities. To observe the maximum phase-dependent interference, the intensities of the sources must be chosen so that the two (single- and three-photon) transition amplitudes become comparable. Further investigation of Eq. (8) shows that if $\Omega_2^{(3)}/q_2^{(3)}=\Omega_2/q_2$ [or $-(\Omega_2/q_2)$] and $\phi=\pi$ (or $\phi=0$),

$$P \propto \frac{1}{\epsilon^2+1}|q_2^{(3)}-q_2|^2 . \tag{27}$$

This equation indicates that the ionization line shape becomes symmetric (Lorentzian) under these conditions. This implies that the continuum part of an AIS is cancelled. Cancellation of the discrete part of an AIS can also be achieved under the condition of $\Omega_2^{(3)}=\Omega_2$. Then,

$$P \propto \frac{\epsilon^2}{\epsilon^2+1}\left|\frac{1}{q_2^{(3)}}-\frac{1}{q_2}\right|^2 . \tag{28}$$

Namely, the ionization line shape becomes flat with the window at $\epsilon=0$. However, the fact that the position of the window is not arbitrary suggests that the atom still remembers where the AIS is, even after the cancellation of the discrete part has been achieved by the phase control.

One may want to ask if it is possible to change the autoionization width by phase control. As one can see from the formalism, this is not the case because the configuration interaction is independent of the external laser fields. It is always there. The autoionization width may be affected only if the intensity effect, which we have derived in Sec. II A 3, is taken into account.

We show now in Figs. 2(a)–2(d) some representative results for selected values of the parameters. The most drastic change is observed when $q_2=-q_2^{(3)}$ [Fig. 2(a)]. The two transition amplitudes interfere 100% destructively or constructively as the relative phase changes from $\phi=0$ (cancellation of the discrete part) to $\phi=\pi$ (cancellation of the continuum part). This is a special case since the conditions for the cancellation of the discrete part and continuum part are satisfied for different values of phase ϕ with the same q, $q^{(3)}$, Ω, and $\Omega^{(3)}$.

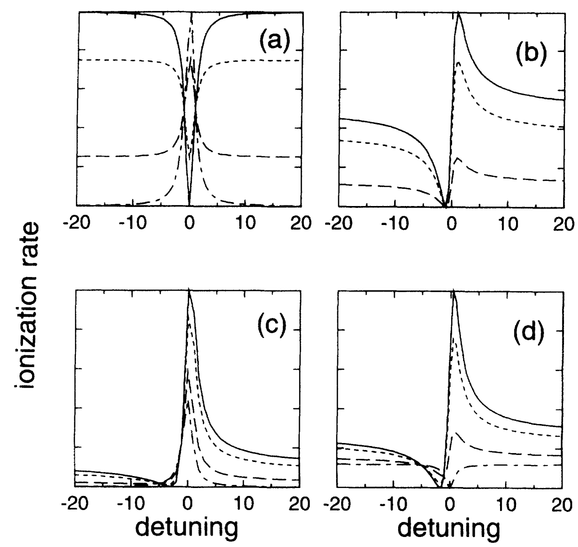

FIG. 2. Change of the autoionization line shape in a weak field as a function of the dimensionless detuning. Relative phase $\phi=0$ (solid line), $\phi=\pi/3$ (dotted), $\phi=2\pi/3$ (dashed), and $\phi=\pi$ (dot-dashed). (a) $\Omega_2^{(3)}/\Omega_2=-1$, $q_2^{(3)}=1$, $q_2=-1$. (b) $\Omega_2^{(3)}/\Omega_2=1$, $q_2^{(3)}=1$, $q_2=1$. (c) $\Omega_2^{(3)}/\Omega_2=5$, $q_2^{(3)}=5$, $q_2=1$. (d) $\Omega_2^{(3)}/\Omega_2=1$, $q_2^{(3)}=5$, $q_2=1$.

If q_2 and $q_2^{(3)}$ have the same sign (not necessarily the same magnitudes), a change of the phase from 0 to π does not cause a dramatic alteration of the line shape as in Fig. 2(b), but still the ionization rate is controllable through ϕ. Given q_2 and $q_2^{(3)}$, which are determined only by the atomic species and its states, one can always choose the laser intensities so that $\Omega_2^{(3)}/q_2^{(3)}=\Omega_2/q_2$ in order to achieve the cancellation of the continuum part of an AIS. An example is given in Fig. 2(c) for $q_2=1$ and $q_2^{(3)}=5$. Partial cancellation is obtained as ϕ changes from 0 to π. At $\phi=\pi$, a complete cancellation of the continuum part is achieved, which is indicated by the symmetric Lorentzian line shape. If, on the other hand, the laser intensities are chosen so that $\Omega_2^{(3)}=\Omega_2$, we achieve the cancellation of the discrete part, leaving only the transition directly into the continuum, as discussed above. An example is given in Fig. 2(d) for $q_2=1$ and $q_2^{(3)}=5$. It is worth stressing that the cancellation of the discrete or continuum part is achievable for any q_2 and $q_2^{(3)}$ by choosing the laser intensities (which is equivalent to choosing the magnitudes of Ω_2 and $\Omega_2^{(3)}$) so as to satisfy the conditions we have given above.

2. Moderate and high intensity

In Sec. III A 1, we have examined the system in terms of the single transition rate approximation. This is valid when external pumping fields are weak in the sense that the configuration interaction V is much stronger than both the single- and three-photon electric dipole interactions, and one may treat the excitation as a weak perturbation. However, when the intensities of pump fields are increased so that $\Omega_2, \Omega_2^{(3)} \gtrsim \Gamma_2$, both configuration interaction and electric dipole interaction must be treated on an equal footing. In other words, the time-independent single rate of the electric dipole interaction is not valid any longer. In this intensity regime, therefore, the time-dependent equations must be solved. One might think that the intensity effects we have described in II A 3 should be taken into account in this intensity region. This may or may not be true, depending on atomic species and states considered. Although there is no difficulty in including the intensity effects in this intensity regime, we will not consider it here and assume that the configuration interaction V is intensity independent. We are interested in the modification of the ionization line shape through the phase. But in a time-dependent calculation, for the ionization line shape to be fully developed [21], the product of the laser-pulse duration T and the autoionization width Γ_2 must be sufficiently large; namely, if $\Gamma_2 T \ll 1$ the spectrum is flat. Therefore, in the following sections, we have employed the values of either $\Gamma_2 T = 5$ or 10, as indicated in each case. During the laser-atom interaction an AIS will be populated, which will then decay into the continuum through configuration interaction. This autoionization decay rate is given by Γ_2. We assume that the laser fields will be turned on at time $t=0$ and last until $t=T$ (square pulse). At a time $t > T$, the ionization yield $Q(t)$ is given by

$$Q(t) = 1 - \sigma_{11}(T) - \sigma_{22}(T) e^{-\Gamma_2(t-T)} . \tag{29}$$

If the ion is collected a long time after the lasers are turned off [in the sense that $\Gamma_2(t-T) \gg 1$], the last term of the above equation may be ignored. This is perhaps most realistic, and the ionization Q in all the graphs in this paper is defined as $Q = 1 - \sigma_{11}(T)$.

First, we show in Fig. 3 how the line shape varies with the atomic parameters, which satisfy the condition for the cancellation of the discrete part of an AIS. In the low intensity region [Fig. 3(a)], the line shape is somehow similar to Fig. 2(d), which is obtained from the transition rate equation. Note, however, that in these figures, the dips for $\phi = \pi$ do not reach zero at the zero detuning, because some atoms are in the excited state just after lasers are turned off, and they will ionize eventually. As the intensity increases [Figs. 3(b) and 3(c)], this tendency is enhanced and deeper dips are observed instead of the peaks. As for the cancellation of the transition directly into the continuum part of an AIS, no significant change is observed [Fig. 4(a)], compared with Fig. 2(c), until the Rabi frequency becomes comparable to the autoionization rate. If the Rabi frequency is comparable to Γ_2 [Fig. 4(b)], the ionization yield for $\phi = \pi$ decreases as the detuning becomes large, while for the rest of the values of ϕ it increases. For some $\Omega_2^{(3)}$ and Ω_2, no significant phase effect is observed, while for the other $\Omega_2^{(3)}$ and Ω_2, the effect is maximized. This is obvious by examining Eq. (8).

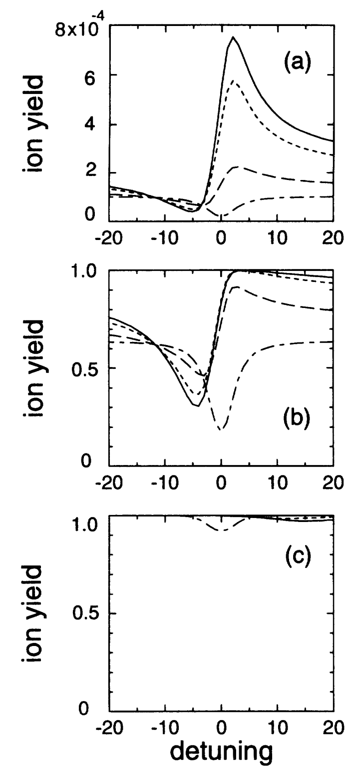

FIG. 3. Cancellation of the discrete part of an autoionizing state at three different Rabi frequencies. $q_2^{(3)} = 5$, $q_2 = 1$, $\Gamma_2 = 5$, and $T = 2$ for all graphs. Relative phase $\phi = 0$ (solid line), $\phi = \pi/3$ (dotted), $\phi = 2\pi/3$ (dashed), and $\phi = \pi$ (dot-dashed). (a) $\Omega_2^{(3)} = 0.01$, $\Omega_2 = 0.01$. (b) $\Omega_2^{(3)} = 1$, $\Omega_2 = 1$. (c) $\Omega_2^{(3)} = 5$, $\Omega_2 = 5$.

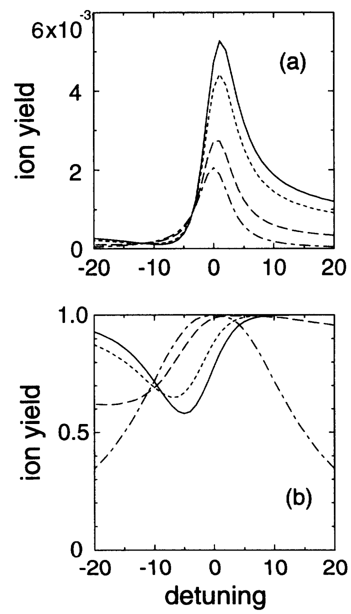

FIG. 4. Cancellation of the continuum part of an autoionizing state at two different Rabi frequencies. $q_2^{(3)} = 5$, $q_2 = 1$, $\Gamma_2 = 5$, and $T = 2$ for both graphs. Relative phase $\phi = 0$ (solid line), $\phi = \pi/3$ (dotted), $\phi = 2\pi/3$ (dashed), and $\phi = \pi$ (dot-dashed). (a) $\Omega_2^{(3)} = 0.05$, $\Omega_2 = 0.01$. (b) $\Omega_2^{(3)} = 5$, $\Omega_2 = 1$.

We should stress that the cancellation of the discrete or continuum part of an AIS can always be realized by adjusting the laser intensities and the relative phase in the moderate and high intensity regimes, as well as the weak intensity region.

If we consider Eq. (2) and choose $\Omega_2^{(3)}$, Ω_2, and ϕ, so that

$$\Omega_2^{(3)}\left[1-\frac{i}{q_2^{(3)}}\right]+e^{i\phi}\Omega_2\left[1-\frac{i}{q_2}\right]=0 ,$$

the second term in Eq. (2) involving σ_{21} vanishes, and the equation now reads

$$\frac{\partial}{\partial t}\sigma_{11}=-\gamma\sigma_{11} . \tag{30}$$

This shows that $|1\rangle$ is completely decoupled from $|2\rangle$. The ionization from $|1\rangle$ shows a completely flat line shape without any windows. This can occur at *any* intensity.

So far we have not included the incoherent ionization channel $\gamma^{(3)}_{\text{incoherent}}$. We now examine the effect of the incoherent channel on the line shape. Since we consider the interference between single- and three-photon ionization, there will always be incoherent, direct three-photon ionization channels from the ground state to the continuum. One of the simplest examples is an $l=3$ continuum reached via the three-photon ionization from an ns^2 ground state of an alkaline-earth-metal atom. This continuum does not interact with a total angular momentum $J=1$ autoionizing state. Thus, the phase-dependent interference for a $J=1$ autoionizing state occurs only through an $l=1$ continuum. The direct ionization to an $l=3$ continuum contributes as a background. Since incoherent channels contribute to the ionization yield as a background, no change of the structure of the spectrum should be observed. Whether the phase-sensitive effects can be detected or not in experiments depends on how much ionization occurs through the incoherent channels and how sensitive a detection system is. In other words, it is a matter of signal to noise ratio. Depending on the atomic states, in many cases the incoherent channel may in fact be much smaller than the coherent channel.

3. *Intensity effects*

The results of the phase-dependent autoionization with the inclusion of intensity effects are presented in this subsection. Since there are many possible combinations of the parameters α', β', α, and β, we show only three examples. The parameters used for the calculations are listed in Table I. Following the argument in Sec. II C 1, only three of those four parameters are independent, and we chose β' as a nonindependent parameter. Results are shown in Figs. 5–7.

Each set of graphs (a)–(d) corresponds to the parameter sets (a)–(d) in Table I. In reality, the relative magnitudes of α', β', α, and β are determined by the atomic states considered. It should be noted that the variation of the phase-dependent line shape, given from (b)–(d), is not observed for one atomic state. In other words, graphs (b)–(d) in each of Figs. 5–7 should be compared with graph (a) in each of Figs. 5–7, which does not include intensity effects, and not with each other. Figure 5(a) corresponds to the case in which the cancellation of the discrete part is achieved at $\phi=\pi$ without intensity effects [identical with Fig. 2(d)]. Depending on the intensity-dependent parameters, which are determined for every atomic state considered, the phase-dependent line shapes are shown in Figs. 5(b)–5(d). It is seen that the ionization line shape changes, depending on the parameters representing the intensity effects. Another example, which shows the cancellation of the continuum part without intensity effects [Fig. 6(a), which is identical with Fig. 2(c)], is shown in Fig. 6. Again, we see the distortion of the spectrum depending on the intensity-dependent parameters [Figs. 6(b)–6(d)]. Figure 7 is another example. For this choice of parameters, the cancellation of neither the discrete nor the continuum part can be achieved without intensity effects [Fig. 7(a)]. The line becomes narrower [Figs. 7(b) and 7(c)] or broader [Fig. 7(d)] when different intensity-dependent parameters are employed. It should be mentioned that the autoionization width $\tilde{\Gamma}_2$ changes because the configuration interaction $\tilde{V}_{c2}$ is now intensity dependent. Therefore, the detuning in all of these graphs has been normalized with respect to the intensity-dependent autoionization width $\tilde{\Gamma}_2$. How much the linewidth varies depends on the intensity-dependent terms such as $\tilde{q}$, $\tilde{\Omega}$, and $\tilde{\Gamma}$, etc.

TABLE I. Parameters for the inclusion of the intensity effects.

Parameter \ Set	(a)	(b)	(c)	(d)
$\alpha' I_1$	0	0.2	−0.4	−0.4
αI_1	0	0.2	0.4	−0.4
βI_1	0	0.2	0.4	−0.4

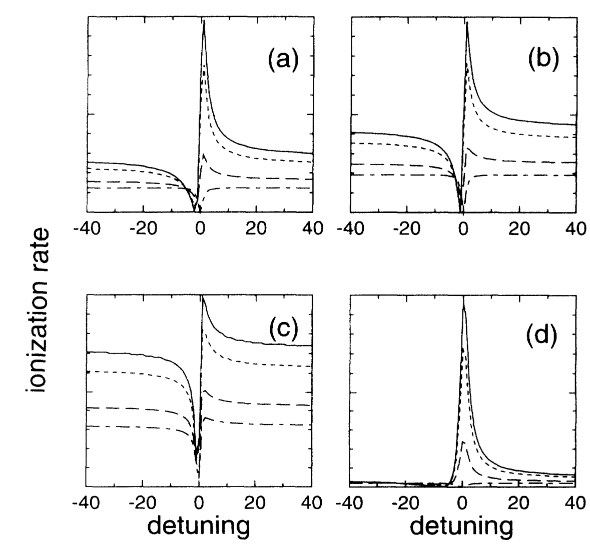

FIG. 5. Variation of the phase-dependent line shape with intensity effects taken into account. Each of (a)–(d) contains graphs at four different relative phase $\phi=0$ (solid line), $\pi/3$ (dotted), $2\pi/3$ (dashed), and π (dot-dashed). $q_2^{(3)}=5$, $q_2=1$, and $\Omega_2^{(3)}/\Omega_2=1$. Intensity-dependent parameters employed in each graph (a)–(d) are listed in Table I.

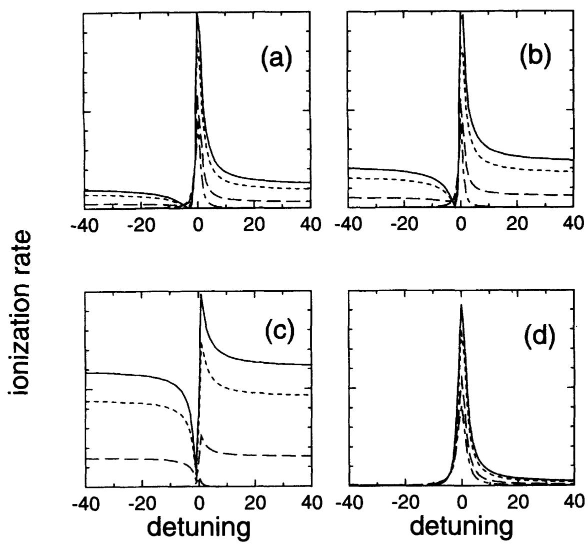

FIG. 6. Variation of the phase-dependent line shape with intensity effects taken into account. Each of (a)–(d) contains graphs at four different relative phase $\phi=0$ (solid line), $\pi/3$ (dotted), $2\pi/3$ (dashed), and π (dot-dashed). $q_2^{(3)}=5$, $q_2=1$, and $\Omega_2^{(3)}/\Omega_2=5$. Intensity-dependent parameters employed in each graph (a)–(d) are listed in Table I.

B. Two autoionizing states

1. *Weak-field limit*

Having investigated the variation of the ionization line shape through the change of the relative phase between the two laser fields in the vicinity of a single AIS $|2\rangle$, we now explore the influence of another AIS $|3\rangle$ lying near $|2\rangle$. This is a natural question since, in reality, it often happens. From Eq. (25), it should be clear that one can turn on and off one of the AIS at will, by choosing Rabi frequencies carefully. We shall not show results here, since from the results in Secs. III A 1 and III A 2, it is clear that results in the weak-field limit are incorporated in those of moderate or high intensity.

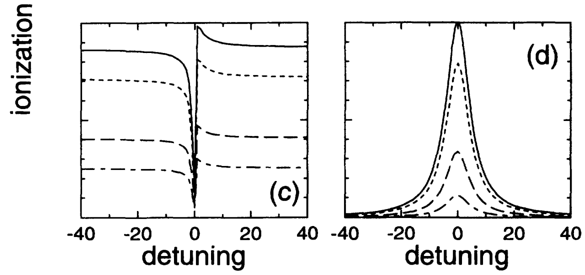

FIG. 7. Variation of the phase-dependent line shape with intensity effects taken into account. Each of (a)–(d) contains graphs at four different relative phase $\phi=0$ (solid line), $\pi/3$ (dotted), $2\pi/3$ (dashed), and π (dot-dashed). $q_2^{(3)}=5$, $q_2=1$, and $\Omega_2^{(3)}/\Omega_2=\frac{1}{2}$. Intensity-dependent parameters employed in each graph (a)–(d) are listed in Table I.

2. *Moderate and high intensity*

We now examine how the ionization spectrum near two AIS's changes as the intensity varies. The level separation S of two AIS's is defined with respect to the larger of the two autoionization widths Γ_2 and Γ_3. To see how the level separation S affects the phase-sensitive spectrum, we have plotted results for two different S (Figs. 8 and 9), each of which contains three graphs at three different Rabi frequencies with $q_2=q_3=5$ and $q_2^{(3)}=q_3^{(3)}=5$. The two peaks of the two AIS are not resolved with this S. In Figs. 8(a)–8(c), S is $0.5\max\{\Gamma_2,\Gamma_3\}$. The separation of the two AIS's still cannot be observed. In Figs. 9(a)–(9c), S is $3.0\max\{\Gamma_2,\Gamma_3\}$, and the Rabi oscillation is prominent in Fig. 9(c).

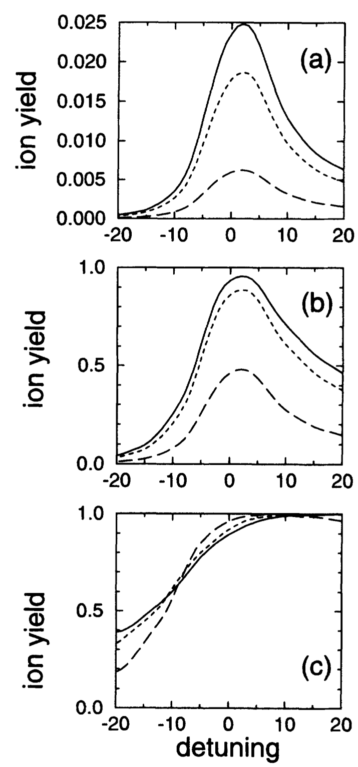

FIG. 8. Ionization line shape in the vicinity of two autoionization states. Separation S between the two autoionization states is $0.5\ \max\{\Gamma_2,\Gamma_3\}$. $q_2^{(3)}=q_2=q_3^{(3)}=q_3=5$, $\Gamma_2=\Gamma_3=5$, and $T=1$. Relative phase $\phi=0$ (solid line), $\pi/3$ (dotted), $2\pi/3$ (dashed), and π (dot-dashed). At $\phi=\pi$, the ionization is completely suppressed in all three graphs. (a) $\Omega_2^{(3)}=\Omega_2=\Omega_3^{(3)}=\Omega_3=0.1$. (b) $\Omega_2^{(3)}=\Omega_2=\Omega_3^{(3)}=\Omega_3=1$. (c) $\Omega_2^{(3)}=\Omega_2=\Omega_3^{(3)}=\Omega_3=5$.

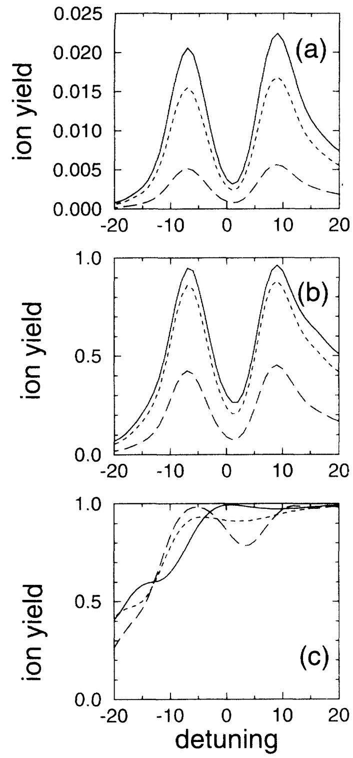

FIG. 9. Ionization line shape in the vicinity of two autoionization states. Separation S between the two autoionization states is $3\max\{\Gamma_2,\Gamma_3\}$. $q_2^{(3)}=q_2=q_3^{(3)}=q_3=5$, $\Gamma_2=\Gamma_3=5$, and $T=1$. Relative phase $\phi=0$ (solid line), $\pi/3$ (dotted), $2\pi/3$ (dashed), and π (dot-dashed). At $\phi=\pi$, the ionization is completely suppressed in all three graphs. (a) $\Omega_2^{(3)}=\Omega_2=\Omega_3^{(3)}=\Omega_3=0.1$. (b) $\Omega_2^{(3)}=\Omega_2=\Omega_3^{(3)}=\Omega_3=1$. (c) $\Omega_2^{(3)}=\Omega_2=\Omega_3^{(3)}=\Omega_3=5$.

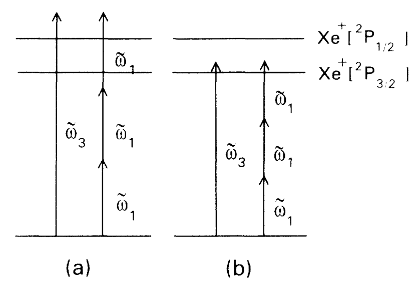

FIG. 10. Schematic diagram of Xe. Two laser frequencies $\tilde{\omega}_1$ and $\tilde{\omega}_3$ have a relation $3\tilde{\omega}_1=\tilde{\omega}_3$. (a) A Xe atom excited in this final energy region can decay into either Xe^+ $P_{3/2}$ or $P_{1/2}$ ionic states. (b) A Xe atom excited in this final energy region may exhibit strong resonance structure (autoionization).

IV. APPLICATION TO Xe

So far we have examined the variation of the autoionization spectrum through phase control by using simple models. We have assumed a single continuum coupled to a single (or two) AIS. This modelling, however, is not adequate for the description of all real atoms quantitatively, since real AIS's are to be described as a superposition of more than one discrete state embedded in general in more than one continuum. Therefore, to simulate the variation of the ionization spectrum of a real atom, we need to carry out more elaborate atomic structure calculations. For this purpose, we have performed calculations for Xe using MQDT (multichannel quantum defect theory, [25,26]). Schematic energy-level diagrams are shown in Fig. 10. We examine the phase effects in two final energy ranges. One is the energy region above the first excited ionic level Xe^+ $[^2P_{1/2}]$ and below the second excited ionic level [Fig. 10(a), which we call case (a)]. A Xe atom excited to this energy region has two possibilities to ionize. One is the $^2P_{3/2}$ and the other is the $^2P_{1/2}$ Xe^+ ionic state. The ratio of the number of neutral atoms decaying to these two final ionic states is defined as a branching ratio, which is determined by the atomic structure.

The other is the energy region between the two ionic states Xe^+ $^2P_{3/2}$ and Xe^+ $^2P_{1/2}$ [Fig. 10(b), which we call case (b)]. In this region, there are many AIS's, most of which are Rydberg states Xe $[^2P_{1/2}]nl$ converging to the Xe^+ $[^2P_{1/2}]$ threshold. A Xe atom excited in this energy region will eventually ionize leaving the Xe^+ $[^2P_{3/2}]$ ion. If the final energy happens to be in the vicinity of states Xe^+ $[^2P_{1/2}]nl$, the ionization is enhanced (autoionization).

Our main interest here is whether the branching ratio of the $^2P_{3/2}$ and $^2P_{1/2}$ ions can be controlled in case (a), and the autoionization line shape can be strongly modified in case (b) due to the interference through the relative phase between the two laser fields. We assume that the two linearly polarized lasers have the frequency relation $\tilde{\omega}_3=3\tilde{\omega}_1$ as before, and employ 5 ns square temporal pulse shape. By the three-photon absorption, the final states can be either $J=1$ or 3 odd-parity states, while by the single-photon absorption, the final states can be $J=1$ odd-parity states only, due to the selection rule of the electric dipole transitions. In jj coupling notation, $J=1$ odd-parity states have five channels, namely $[^2P_{1/2}]d_{3/2}$, $[^2P_{3/2}]d_{5/2}$, $[^2P_{3/2}]d_{3/2}$, $[^2P_{1/2}]s_{1/2}$, and $[^2P_{3/2}]s_{1/2}$. $J=3$ odd-parity states have six channels which are given by $[^2P_{1/2}]d_{5/2}$, $[^2P_{3/2}]d_{3/2}$, $[^2P_{3/2}]d_{5/2}$, $[^2P_{1/2}]g_{7/2}$, $[^2P_{3/2},]g_{9/2}$, and $[^2P_{3/2}]g_{7/2}$. ($[^2P_{1/2}]$ or $[^2P_{3/2}]$ are the designations for the ionic core $5p^5$, and $d_{3/2}$, etc., are the designations of the outmost electron.)

Given the quantum defects μ_α's and transformation matrix $U_{\alpha i}$, we can expand the final-state wave function in terms of spherical harmonics Y_{lm_l}. (For the application of MQDT to the multiphoton processes and the details of the notations used here, the reader is referred to [26].) Namely,

$$|f_{m_s,m_{J_c},J_c}(\hat{k},r)\rangle=\sum_{l,m_l} i^l e^{-i\delta_l} Y^*_{lm_l}(\hat{k}) \sum_{j,J,\alpha} e^{-i\pi\mu_\alpha}(\alpha|J_cjJM_J)(J_cjJM_J|J_cm_{J_c}jm_j)(J_cm_{J_c}jm_j|lm_lsm_s)|\alpha\rangle\ , \tag{31}$$

where δ_l is the Coulomb phase shift and $\hat{k}=(\theta,\varphi)$ characterizes the direction of the photoelectron with respect to the laser polarization axis for linear polarization. The N-photon partial ionization amplitude is now written as

$$M^{(N)}(\hat{k})[m_s,m_{J_c},J_c]=\sum_{l,m_l,j,J,\alpha} i^l(-1)^{1/2-m_j-j+J_c-M_J}e^{i\delta_l+i\pi\mu_\alpha}Y_{lm_l}(\hat{k})[(2j+1)(2J+1)]^{1/2} \times \begin{pmatrix} l & s & j \\ m_l & m_s & -m_j \end{pmatrix}\begin{pmatrix} j & J_c & J \\ m_j & m_{J_c} & -M_J \end{pmatrix} Z_{i\alpha}D_\alpha^{(N)} . \quad (32)$$

The differential ionization rate under the presence of two fields with the intensity I_1 and I_3 (both in W/cm^2) is given by

$$\frac{dR}{d\Omega}=\sum_{m_s,m_{J_c}} |n_1M^{(1)}(\hat{k})[m_s,m_{J_c},J_c]\sqrt{I_3} + e^{i\phi}n_3M^{(3)}(\hat{k})[m_s,m_{J_c},J_c]\sqrt{I_1^3}\,|^2 , \quad (33)$$

where $n_1=0.767$ and $n_3=5.47\times10^{-18}$ are the conversion factors to the appropriate units (s^{-1}). The total ionization rate R is now obtained by integrating the calculated differential ionization rate $dR/d\Omega$ over the solid angle Ω. Obviously, the interference due to the two laser fields occurs between the states with the *same* Y_{lm_l} for R and between *any* states with *any* Y_{lm_l} for $dR/d\Omega$ [3]. It should be clear at this point that to consider the interference by the two laser beams at $\tilde{\omega}_1$ and $\tilde{\omega}_3$, one must further decompose every channel mentioned above (five channels for $J=1$ and six channels for $J=3$) into a superposition of the spherical harmonics. The number of possible Y_{lm_l} exceeds 10 for $J=3$. It is far from obvious at this stage whether the phase-dependent interference will be observable or not.

First, we discuss bound-continuum transitions [case (a)]. In this case, the ionization occurs to either $^2P_{3/2}$ or $^2P_{1/2}$ ionic states, and the ratio of these two yields gives the branching ratio, which is defined as $B\equiv(P_{1/2}$ ion yield)/($P_{3/2}$ ion yield). Under the presence of a single laser field, this branching ratio is determined from the atomic structure and the number of the photons involved, and does not depend on laser intensities. The frequency dependence of the branching ratio B for each single- and three-photon ionization from the ground state of Xe is shown in Fig. 11. Note that the branching ratio in three-photon ionization reveals structure due to the intermediate states lying near the two-photon energy levels. The simple explanation of the peaks near the 135 000 cm^{-1} is that, since there are two near-resonant states with $P_{1/2}$ ion core at the two-photon energy range, an atom excited with this photon energy is likely to have $P_{1/2}$ ion character; therefore the branching ratio becomes large in this range. The branching ratio by single-photon ionization does not have structure, simply because there are no near-resonant effects.

We now discuss what will happen when an atom is exposed to two fields with a well-defined relative phase. Although the phase effects should be observed at any ϕ, we have chosen $\phi=0$ and $\phi=\pi$ only for demonstration, and not because maximum phase effects are observed at these ϕ's. The final states consist of many partial waves with $Y'_{lm}s$ complex phase shifts. It is not *a priori* obvious at which ϕ the maximum (or minimum) interference through the phase will occur. In Fig. 12, the laser intensities are chosen so that the ionization by single-photon absorption is much stronger than by three-photon ionization, and the phase effects are very small. Some deviation from the background ionization is observed when the three-photon ionization is enhanced by near resonance at the two-photon absorption level. In the energy range of Fig. 12, the three-photon process comes near resonance with several states as the photon frequency $\tilde{\omega}_1$ is scanned. We list below those resonant states, which lie around the two-photon energy region $2\tilde{\omega}_1$, together with the final energy $3\tilde{\omega}_1$ reached by the resonant photon frequency in each case [27].

State	$3\tilde{\omega}_1$ (cm^{-1})
$[^2P_{3/2}]6p,j=2$	117 180
$[^2P_{3/2}]6p,j=2$	118 818
$[^2P_{3/2}]6p,j=0$	120 180
$[^2P_{3/2}]7p,j=2$	132 528
$[^2P_{3/2}]7p,j=2$	133 031
$[^2P_{3/2}]7p,j=0$	133 265
$[^2P_{1/2}]6p',j=2$	133 745
$[^2P_{1/2}]6p',j=0$	134 790
$[^2P_{3/2}]4f,j=2$	136 275
$[^2P_{3/2}]4f,j=2$	136 367

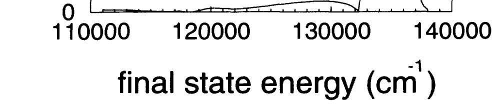

FIG. 11. Branching ratio of Xe as a function of final-state energy. Branching ratio is defined in the text. Branching ratio by three-photon ($3\tilde{\omega}_1$) absorption (solid line) and single-photon ($\tilde{\omega}_3$) absorption (dashed line) are shown. Note that each plot has been obtained in the presence of a single laser field (either $\tilde{\omega}_1$ or $\tilde{\omega}_3$).

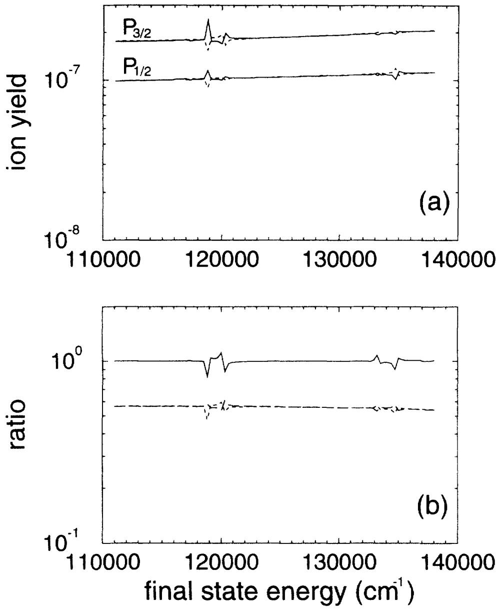

FIG. 12. Ionization yield and branching ratio as a function of final-state energy in the presence of two laser fields. 5 ns square pulse has been employed. $I_1 = 10^8$ W/cm^2 and $I_3 = 10$ W/cm^2. (a) Ionization yield of $P_{3/2}$ ion and $P_{1/2}$ ion. Relative phase is set to $\phi = 0$ (solid line) or $\phi = \pi$ (dashed line). (b) Branching ratio at $\phi = 0$ (dotted line) and $\phi = \pi$ (dashed line). In (b), the ratio of branching ratios at $\phi = 0$ and $\phi = \pi$ has also been plotted (solid line). The bigger deviation of this value from 1 indicates the bigger phase effects.

Figure 13 shows a little more interference, with the three-photon laser intensity increased by one order of magnitude. The deviation from the background, however, is observed again only in the vicinity of the resonant energy we have listed above. This indicates that the transitions through the three-photon absorption are still weaker than the single-photon process, unless the three-photon process is enhanced through resonance. Slight variation of the ion yield through the phase at the nonresonant energy region begins to be seen. But most of the peaks in Fig. 13 are due to the resonance effect. (The divergence at resonances has been truncated.) An exception is the peak at 135 100 cm^{-1}. This energy is about 300 cm^{-1} away from the nearest resonant state. Figure 14 shows the most interesting features. When the final energy is near resonant, no phase effects are observed, since the ionization through the three-photon process becomes dominant over the single-photon process. Therefore, strong interference is seen when $2\tilde{\omega}_1$ is away from any levels (Fig. 14). The peaks of the branching ratio appear when no resonance occurs, and the branching ratio becomes as large as 10. These results indicate that the branching ratio of the $^2P_{3/2}$ and $^2P_{1/2}$ ion can be significantly controlled by manipulating the relative phase of the laser fields without changing the laser intensities. We have also calculated the photoelectron angular distribution at a final energy 133 800 cm^{-1} as an example (Fig. 15). As we have seen in the total ionization yield, the strong phase dependence is found in the photoelectron angular distribution as well. Figs. 15(a)–15(d) are in increasing order of the laser intensity I_1 with fixed I_3. When I_1 is not sufficiently strong, the total angular distribution is dominated by that of the single-photon process

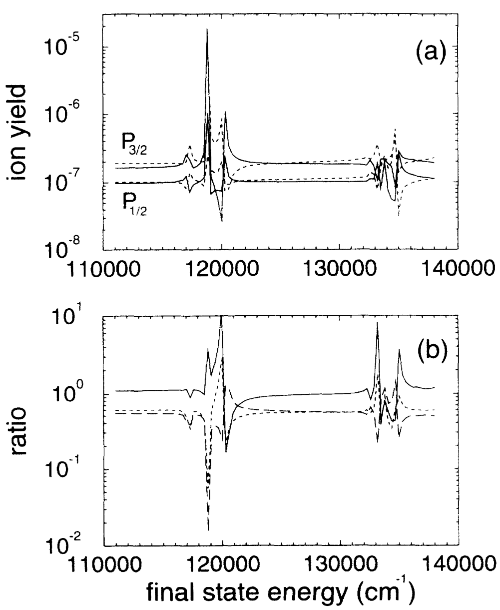

FIG. 13. Same as Fig. 12, but at $I_1 = 10^9$ W/cm^2. Pulse duration and I_3 are kept to the same values as those in Fig. 12.

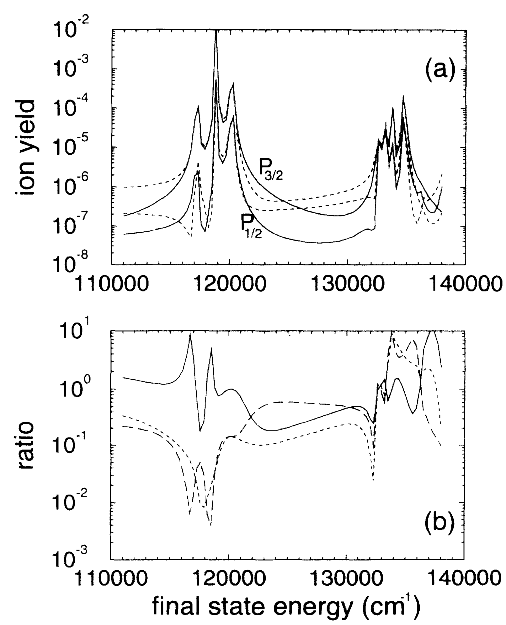

FIG. 14. Same as Fig. 12, but at $I_1 = 10^{10}$ W/cm^2. Pulse duration and I_3 are kept to the same values as those in Fig. 12.

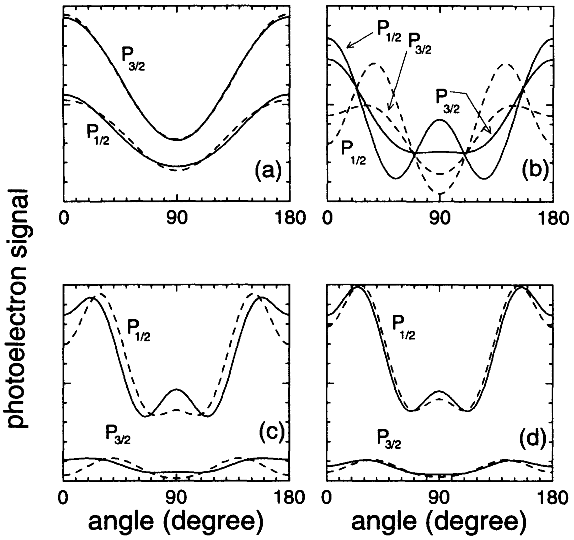

FIG. 15. Photoelectron angular distribution (PAD) from the final energy 133 800 cm^{-1} under the presence of two laser fields at different relative phase $\phi=0$ (solid line) and $\phi=\pi$ (dotted line). After the emission of a photoelectron, a Xe core is left in either $P_{3/2}$ or $P_{1/2}$ ionic states of Xe$^+$. PAD's corresponding to each $P_{3/2}$ or $P_{1/2}$ ionic state are plotted separately and indicated in each graph. $I_3=10$ W/cm^2 [fixed through (a) to (d)]. (a) $I_1=10^8$ W/cm^2. (b) $I_1=10^9$ W/cm^2. (c) $I_1=5\times10^9$ W/cm^2. (d) $I_1=10^{10}$ W/cm^2.

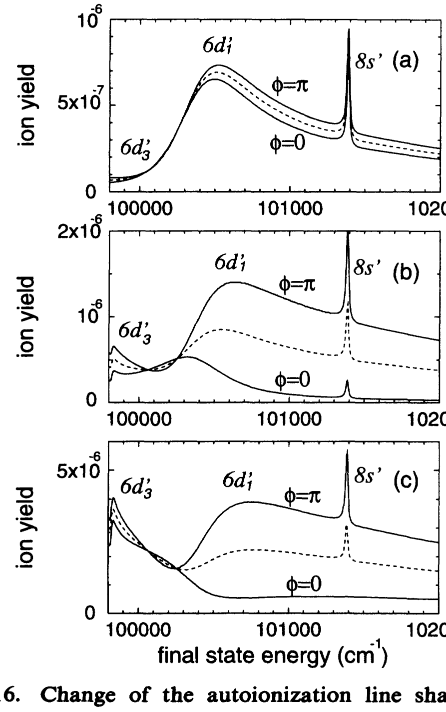

FIG. 16. Change of the autoionization line shape of Xe through the relative phase ϕ of two laser fields. $I_3=10$ W/cm^2 [fixed through (a) to (c)]. 5 ns square pulse. (a) $I_1=10^9$ W/cm^2. (b) $I_1=5\times10^9$ W/cm^2. (c) $I_1=10^{10}$ W/cm^2. Dashed line corresponds to the incoherent ionization by the two fields. $8s'$, $6d'_1$, and $6d'_3$ in the figures correspond to the autoionizing states $[P_{1/2}]8s_{1/2}$ $(J=1)$, $[P_{1/2}]6d_{3/2}$ $(J=1)$, and $[P_{1/2}]6d_{5/2}$ $(J=3)$, respectively.

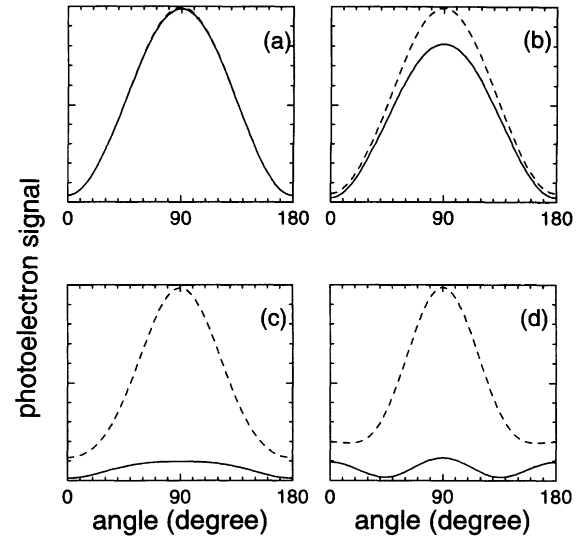

FIG. 17. PAD from the autoionization peak $8s'$ of Xe under the presence of two laser fields at two different relative phase $\phi=0$ (solid line) and $\phi=\pi$ (dotted line). $I_3=10$ W/cm^2 [fixed through (a) to (d)]. 5 ns square pulse. (a) $I_1=10^8$ W/cm^2. (b) $I_1=10^9$ W/cm^2. (c) $I_1=5\times10^9$ W/cm^2. (d) $I_1=10^{10}$ W/cm^2.

[Fig. 15(a)]. As I_1 increases, two (single- and three-photon) transition processes interfere strongly with each other, and the strong variation of the angular distribution is seen [Fig. 15(b)]. Further increase of I_1 causes the dominance of the three-photon process, and the phase-dependent interference decreases [Figs. 15(c) and 15(d)].

We consider now the phase effects in the autoionization region [case (b)]. The same procedure has been applied: We expand the final open channels as described above. Ionization spectra are plotted in Figs. 16(a)–16(c), again in increasing order of I_1 with fixed I_3. The feature of Fig. 16(a) comes from the single-photon autoionization because the three-photon transition amplitude is too weak. As the three-photon laser intensity increases, the phase effects begin to appear [Fig. 16(b)]. The line shape, however, still resembles that of the single-photon process. The further increase of the three-photon laser intensity reveals the more interesting line shape. Figure 16(c) demonstrates that the autoionization line shape is significantly changed by the relative phase of the lasers. The sharp peak at 101 390 cm^{-1} ($8s'$) is enhanced (dehanced) as the relative phase changes. We have also plotted the photoelectron angular distribution corresponding to the autoionization peak $8s'$ (Fig. 17). The significant variation of the angular distribution is found again in the autoionization region.

V. SUMMARY AND CONCLUSIONS

By using a simple model, we have shown that the line shape of an isolated AIS is significantly altered under the presence of a laser field of frequency $\tilde{\omega}_1$ and its third harmonic $\tilde{\omega}_3=3\tilde{\omega}_1$, as a function of their relative phase. A careful choice of the laser intensities and the phase leads to the cancellation of the discrete or a continuum part of an AIS. As the laser intensity I_1 at $\tilde{\omega}_1$ increases, intensity effects, which cause an additional Raman-type radiative coupling between the discrete and continuum part of an AIS as well as the nonradiative configuration interaction, emerge. This effect has been examined within the single-rate approximation. A few representative illustrative intensity effects have been presented, and it has been seen that, depending on the strength and the sign of this Raman-type coupling transition amplitude, intensity effects might significantly distort the autoionization line shape compared with the one at a lower intensity, which does not exhibit intensity effects. To investigate how much an autoionization line shape is affected by another AIS lying nearby, we have performed model calculations with two AIS's, both of which are coupled to a bound state (usually a ground state) simultaneously by a three- and a single-photon transition with well defined phase difference. We have also carried out MQDT calculations on Xe under the presence of two laser fields. Two energy regions have been examined. One is above the first excited state of Xe^+. The other is between the ground and first excited state of Xe^+. In both regions, significant phase effects have been found in terms of the photoelectron angular distributions as well as the ionization yield. The photon energies and intensities employed in these calculations for Xe are accessible experimentally by current laser systems. We believe that our model as well as our realistic calculations support the idea that these effects are rather general and should be found in most systems, provided that the frequency of the radiation and the proximity to excited states are chosen judiciously.

ACKNOWLEDGMENT

This work was supported by the NSF under Grant No. PHY-9215229 and the DOE under Grant No. DE-FG03-87ER60504.

APPENDIX A

We present the derivation of the density-matrix equations, which describe the atomic dynamics of a two (one bound state $|1\rangle$ and one discrete state $|2\rangle$ embedded in a continuum $|c\rangle$, i.e., an AIS) level system coupled by a single photon with the laser frequency $\tilde{\omega}_3$ as well as by three photons with the laser frequency $\tilde{\omega}_1$ with $3\tilde{\omega}_1=\tilde{\omega}_3$. These two atomic states $|1\rangle$ and $|2\rangle$ have energies $\hbar\omega_1$ and $\hbar\omega_2$. For simplicity, we do not include the intensity effects in this derivation. The generalization to the two-AIS case is straightforward. Our total atomic Hamiltonian is

$$H=H_0+D^{(3)}+\mathcal{D}+V\ , \tag{A1}$$

where H_0 is the unperturbed atomic Hamiltonian, $D^{(3)}$ is an effective three-photon $(3\tilde{\omega}_1)$ electric dipole operator, $\mathcal{D}$ an electric dipole operator $(\tilde{\omega}_3=3\tilde{\omega}_1)$, and V is a configuration interaction. Then, starting with the equation of motion of the density operator ρ,

$$i\hbar\dot{\rho}=[H_0+D^{(3)}+\mathcal{D}+V,\rho]\ , \tag{A2}$$

we obtain

$$\dot{\rho}_{11}=-i\hbar^{-1}\left[(D^{(3)}_{12}+\mathcal{D}_{12})\rho_{21}+\sum_c (D^{(3)}_{1c}+\mathcal{D}_{1c})\rho_{c1}-\text{c.c.}\right]\ , \tag{A3}$$

$$\dot{\rho}_{22}=-i\hbar^{-1}\left[(D^{(3)}_{21}+\mathcal{D}_{21})\rho_{12}+\sum_c V_{2c}\rho_{c2}-\text{c.c.}\right]\ , \tag{A4}$$

$$\dot{\rho}_{21}=-i\omega_{21}\rho_{21}-i\hbar^{-1}\left[(D^{(3)}_{21}+\mathcal{D}_{21})\rho_{11}+\sum_c V_{2c}\rho_{c1}-\rho_{22}(D^{(3)}_{21}+\mathcal{D}_{21})-\sum_c \rho_{2c}(D^{(3)}_{c1}+\mathcal{D}_{c1})\right]\ , \tag{A5}$$

$$\dot{\rho}_{c1}=-i\omega_{c1}\rho_{c1}-i\hbar^{-1}\left[(D^{(3)}_{c1}+\mathcal{D}_{c1})\rho_{11}+\sum_c V_{c2}\rho_{21}-\rho_{c2}(D^{(3)}_{21}+\mathcal{D}_{21})\right]\ , \tag{A6}$$

$$\dot{\rho}_{c2}=-i\omega_{c2}\rho_{c2}-i\hbar^{-1}\left[(D^{(3)}_{c1}+\mathcal{D}_{c1})\rho_{12}+\sum_c V_{c2}\rho_{22}-\rho_{c1}(D^{(3)}_{12}+\mathcal{D}_{12})\right]\ , \tag{A7}$$

where $D^{(3)}_{ij}$ and $\mathcal{D}_{ij}$ denote the single- and effective three-photon dipole matrix elements between $|i\rangle$ and $|j\rangle$, respectively, and $\omega_{ij}\equiv\omega_i-\omega_j$. $\sum_c$ represents the integration as well as the summation over all possible virtual (bound and continuum) states. Introducing slowly varying amplitudes, namely, $\rho_{ii}=\sigma_{ii}$ $(i=1,2)$, $\rho_{21}=\sigma_{21}e^{-i3\tilde{\omega}_1 t}$, $\rho_{c1}=\sigma_{c1}e^{-i3\tilde{\omega}_1 t}$, and $\rho_{c2}=\sigma_{c2}$, followed by the rotating-wave approximation, we obtain

$$\dot{\sigma}_{11}=-i\hbar^{-1}\left[(\mu^{(3)}_{12}\varepsilon_1^3+\mu_{12}\varepsilon_3e^{i\phi})\sigma_{21}+\sum_c(\mu^{(3)}_{1c}\varepsilon_1^3+\mu_{1c}\varepsilon_3e^{i\phi})\sigma_{c1}-\text{c.c.}\right]\ , \tag{A8}$$

$$\dot{\sigma}_{22}=-i\hbar^{-1}\left[(\mu^{(3)}_{21}\varepsilon_1^{*3}+\mu_{21}\varepsilon_3^{*}e^{-i\phi})\sigma_{12}+\sum_c V_{2c}\sigma_{c2}-\text{c.c.}\right]\ , \tag{A9}$$

$$\dot{\sigma}_{21}=i(3\tilde{\omega}_1-\omega_{21})\sigma_{21}-i\hbar^{-1}\left[(\mu^{(3)}_{21}\varepsilon_1^{*3}+\mu_{21}\varepsilon_3^{*}e^{-i\phi})(\sigma_{11}-\sigma_{22})+\sum_c V_{2c}\sigma_{c1}-\sum_c\left[\mu^{(3)}_{c1}\varepsilon_1^{*3}+\mu_{c1}\varepsilon_3^{*}e^{i\phi}\right]\sigma_{2c}\right]\ , \tag{A10}$$

$$\dot{\sigma}_{c1}=i(3\tilde{\omega}_1-\omega_{c1})\sigma_{c1}-i\hbar^{-1}[(\mu_{c1}^{(3)}\varepsilon_1^{*3}+\mu_{c1}\varepsilon_3^{*}e^{-i\phi})\sigma_{11}+V_{c2}\sigma_{21}-(\mu_{21}^{(3)}\varepsilon_1^{*3}+\mu_{21}\varepsilon_3^{*}e^{-i\phi})\sigma_{c2}]\ , \quad (A11)$$

$$\dot{\sigma}_{c2}=-i\omega_{c2}\sigma_{c2}-i\hbar^{-1}[(\mu_{c1}^{(3)}\varepsilon_1^{*3}+\mu_{c1}\varepsilon_3^{*}e^{-i\phi})\sigma_{12}+V_{c2}\sigma_{22}-(\mu_{12}^{(3)}\varepsilon_1^{3}+\mu_{12}\varepsilon_3e^{i\phi})\sigma_{c1}]\ . \quad (A12)$$

The time derivative of the last two equations may be ignored by applying the adiabatic approximation. Then,

$$\sigma_{c1}\simeq\frac{1}{\hbar(3\tilde{\omega}_1-\omega_{c1})+i\epsilon}[(\mu_{c1}^{(3)}\varepsilon_1^{*3}+\mu_{c1}\varepsilon_3^{*}e^{-i\phi})\sigma_{11}+V_{c2}\sigma_{21}]\ , \quad (A13)$$

$$\sigma_{c2}\simeq\frac{-1}{\hbar\omega_{c2}-i\epsilon}[(\mu_{c1}^{(3)}\varepsilon_1^{*3}+\mu_{c1}\varepsilon_3^{*}e^{-i\phi})\sigma_{12}+V_{c2}\sigma_{22}]\ , \quad (A14)$$

where ϵ is a small positive number and $\lim_{\epsilon\to+0}$ should be taken in the end wherever ϵ appears. Substituting these two equations,

$$\dot{\sigma}_{11}=2\hbar^{-1}\mathrm{Im}\left[\sum_c\frac{|\mu_{1c}^{(3)}\varepsilon_1^3+\mu_{1c}\varepsilon_3e^{i\phi}|^2}{\hbar(3\tilde{\omega}_1-\omega_{c1})}\sigma_{11}\right]+2\hbar^{-1}\mathrm{Im}\left[(\mu_{12}^{(3)}\varepsilon_1^3+e^{i\phi}\mu_{12}\varepsilon_3)+\sum_c\frac{(\mu_{1c}^{(3)}\varepsilon_1^3+\mu_{1c}\varepsilon_3e^{i\phi})V_{c2}}{\hbar(3\tilde{\omega}_1-\omega_{c1})}\sigma_{21}\right]\ . \quad (A15)$$

Defining

$$\Omega_2^{(3)}\equiv\frac{\mu_{12}^{(3)}\varepsilon_1^3}{\hbar}+\mathrm{P}\sum_c\frac{\mu_{1c}^{(3)}\varepsilon_1^3V_{c2}}{\hbar^2(3\tilde{\omega}_1-\omega_{c1})}\ , \quad (A16)$$

$$q_2^{(3)}\equiv\frac{\Omega_2^{(3)}}{\pi\hbar^{-2}(\mu_{1c}^{(3)}\varepsilon_1^3V_{c2})_{\omega_c=\omega_1+3\tilde{\omega}_1}}\ , \quad (A17)$$

$$\Omega_2\equiv\frac{\mu_{12}\varepsilon_3}{\hbar}+\mathrm{P}\sum_c\frac{\mu_{1c}\varepsilon_3V_{c2}}{\hbar^2(3\tilde{\omega}_1-\omega_{c1})}\ , \quad (A18)$$

$$q_2\equiv\frac{\Omega_2}{\pi\hbar^{-2}(\mu_{1c}\varepsilon_3V_{c2})_{\omega_c=\omega_1+3\tilde{\omega}_1}}\ , \quad (A19)$$

$$S_1-\frac{i}{2}\gamma\equiv\hbar^{-2}\sum_c\frac{|\mu_{1c}^{(3)}\varepsilon_1^3+\mu_{1c}\varepsilon_3e^{i\phi}|^2}{3\tilde{\omega}_1-\omega_{c1}+i\epsilon}\ , \quad (A20)$$

in the last equation, the ac Stark shift S_1 of state $|1\rangle$ has been introduced. We now have

$$\dot{\sigma}_{11}=-\gamma\sigma_{11}+2\,\mathrm{Im}\left\{\left[\Omega_2^{(3)}\left[1-\frac{i}{q_2^{(3)}}\right]+e^{i\phi}\Omega_2\left[1-\frac{i}{q_2}\right]\right]\sigma_{21}\right\}\ . \quad (A21)$$

Similarly,

$$\dot{\sigma}_{22}=-\Gamma_2\sigma_{22}-2\,\mathrm{Im}\left\{\left[\Omega_2^{(3)}\left[1+\frac{i}{q_2^{(3)}}\right]+e^{i\phi}\Omega_2\left[1+\frac{i}{q_2}\right]\right]\sigma_{21}\right\}\ , \quad (A22)$$

with

$$S_2-\frac{i}{2}\Gamma_2=\hbar^{-2}\sum_c\frac{|V_{c2}|^2}{(3\tilde{\omega}_1-\omega_{c1})+i\epsilon} \quad (A23)$$

and

$$\dot{\sigma}_{21}=[i\delta_2-\tfrac{1}{2}(\Gamma_2+\gamma)]\sigma_{21}-i\left[\Omega_2^{(3)}\left[1-\frac{i}{q_2^{(3)}}\right]+e^{-i\phi}\Omega_2\left[1-\frac{i}{q_2}\right]\right]\sigma_{11}+i\left[\Omega_2^{(3)}\left[1+\frac{i}{q_2^{(3)}}\right]+e^{-i\phi}\Omega_2\left[1+\frac{i}{q_2}\right]\right]\sigma_{22}\ , \quad (A24)$$

where $\delta_2\equiv3\tilde{\omega}_1-[(\omega_2+S_2)-(\omega_1+S_1)]\equiv3\tilde{\omega}_1-(\bar{\omega}_2-\bar{\omega}_1)$.

APPENDIX B

A derivation of the photoionization rate from a bound state $|1\rangle$ to the double AIS is similar to that for the single AIS case, which has been given in the text. Starting from the full set of the density-matrix equations, and assuming the weak-field limit which implies $\sigma_{11}(t)\sim1$, $\sigma_{22}(t)=\sigma_{33}(t)\simeq0$, and $\dot{\sigma}_{21}=\dot{\sigma}_{31}=\dot{\sigma}_{32}=0$, we obtain

$$[-i\delta_2+\tfrac{1}{2}(\gamma+\Gamma_2)]\sigma_{21}=-i\Omega_2\left[1-\frac{i}{q_2}\right]\ , \quad (B1)$$

$$[-i\delta_3+\tfrac{1}{2}(\gamma+\Gamma_3)]\sigma_{31}=-i\Omega_3\left[1-\frac{i}{q_3}\right]\ . \quad (B2)$$

The term with σ_{32} has been ignored in the lowest order approximation. Solving these equations and substituting into the equation for $\dot{\sigma}_{11}$, we obtain

$$\dot{\sigma}_{11}\simeq-\gamma+2\,\mathrm{Im}\left[\frac{-i(\Omega_2)^2\left[1-\frac{i}{q_2}\right]^2(-i\delta_3+\Gamma_3/2)}{(-i\delta_2+\Gamma_2)(-i\delta_3+\Gamma_3/2)}\right]+2\,\mathrm{Im}\left[\frac{-i(\Omega_3)^2\left[1-\frac{i}{q_3}\right]^2(-i\delta_2+\Gamma_2/2)}{(-i\delta_2+\Gamma_2)(-i\delta_3+\Gamma_3/2)}\right]\ . \quad (B3)$$

After some algebra,

$$\dot{\sigma}_{11} = -\gamma + 2(\Omega_2)^2 \mathrm{Im} \left[\frac{i\left(1-\frac{i}{q_2}\right)^2 (-i\delta_3+\Gamma_3/2)\{\delta_2\delta_3 - i(\delta_2\Gamma_3/2+\delta_3\Gamma_2/2)\}}{(\delta_2\delta_3)^2+(\delta_2\Gamma_3/2+\delta_3\Gamma_2/2)^2} \right]$$

$$+2(\Omega_3)^2 \mathrm{Im} \left[\frac{i\left(1-\frac{i}{q_3}\right)^2 (-i\delta_2+\Gamma_2/2)\{\delta_2\delta_3 - i(\delta_2\Gamma_3/2+\delta_3\Gamma_2/2)\}}{(\delta_2\delta_3)^2+(\delta_2\Gamma_3/2+\delta_3\Gamma_2/2)^2} \right] . \quad \text{(B4)}$$

Defining the dimensionless detunings $\epsilon_i \equiv \delta_i/(\Gamma_i/2)$ and noting that $\Omega_i^2 = q_i^2\Gamma_i\gamma/4$ $(i=2,3)$, we finally obtain

$$\dot{\sigma}_{11} = -\gamma \frac{(q_2\epsilon_3+q_3\epsilon_2+\epsilon_2\epsilon_3)^2}{(\epsilon_2\epsilon_3)^2+(\epsilon_2+\epsilon_3)^2} . \quad \text{(B5)}$$

[1] Takashi Nakajima and P. Lambropoulos, Phys. Rev. Lett. **70**, 1081 (1993).

[2] Ce Chen, Yi-Yian Yin, and D. S. Elliott, Phys. Rev. Lett. **64**, 507 (1990); Ce Chen and D. S. Elliott, *ibid.* **65**, 1737 (1990).

[3] Yi-Yian Yin, Ce Chen, and D. S. Elliott, Phys. Rev. Lett. **69**, 2353 (1992).

[4] Takashi Nakajima, P. Lambropoulos, S. Cavalieri, and M. Matera, Phys. Rev. A **46**, 7315 (1992).

[5] H. G. Muller, P. H. Bucksbaum, D. W. Schumacher, and A. Zavriyev, J. Phys. B **23**, 2761 (1990).

[6] R. M. Potvliege and Philip H. G. Smith, J. Phys. B **24**, L641 (1991); **25**, 2501 (1992).

[7] A. Szöke, K. C. Kulander, and J. N. Bardsley, J. Phys. B **24**, 3165 (1991).

[8] Kenneth J. Schafer and Kenneth C. Kulander, Phys. Rev. A **45**, 8026 (1992).

[9] M. Shapiro, J. W. Hepburn, and P. Brumer, Chem. Phys. Lett. **149**, 451 (1988).

[10] Seung Min Park, Shao-Ping Lu, and Robert J. Gordon, J. Chem. Phys. **94**, 8622 (1991); Shao-Ping Lu, Seung Min Park, Yongjin Xie, and Robert J. Gordon, *ibid.* **96**, 6613 (1992).

[11] A. D. Bandrauk, J. M. Gauthier, and J. F. McCann, Chem. Phys. Lett. **200**, 399 (1992).

[12] D. J. Tannor and S. A. Rice, J. Chem. Phys. **83**, 5013 (1985).

[13] N. F. Scherer, A. J. Ruggiero, M. Du, and G. R. Fleming, J. Chem. Phys. **93**, 856 (1990).

[14] D. Normand, L. A. Lompré, and C. Cornaggia, J. Phys. B **25**, L497 (1992).

[15] M. Shapiro and P. Brumer, J. Chem. Phys. **98**, 201 (1993).

[16] C. Asaro, P. Brumer, and M. Shapiro, Phys. Rev. Lett. **60**, 1634 (1988).

[17] Zhidang Chen, P. Brumer, and M. Shapiro, Chem. Phys. Lett. **198**, 498 (1992); **98**, 6843 (1993).

[18] R. J. Gordon, Shao-Ping Lu, Seung Min Park, Karen Trentelman, Yongjin Xie, Langchi Zhu, Ashok Kumar, and William J. Meath, J. Chem. Phys. **98**, 9481 (1993).

[19] E. Charron, A. Giusti-Suzor, and F. H. Mies, Phys. Rev. Lett. **71**, 692 (1993).

[20] Young Soon Kim and P. Lambropoulos, Phys. Rev. A **29**, 3159 (1984).

[21] P. Lambropoulos and P. Zoller, Phys. Rev. A **24**, 379 (1981).

[22] S. N. Dixit and P. Lambropoulos, Phys. Rev. A **27**, 861 (1983).

[23] G. Alber and P. Zoller, Phys. Rev. A **26**, 1373 (1982).

[24] U. Fano, Phys. Rev. **124**, 1866 (1961).

[25] M. J. Seaton, Proc. Phys. Soc. London **88**, 801 (1966); Rep. Prog. Phys. **46**, 167 (1983).

[26] A. L'Huillier, X. Tang, and P. Lambropoulos, Phys. Rev. A **39**, 1112 (1989).

[27] C. E. Moore, *Atomic Energy Levels,* Natl. Bur. Stand. (U.S.) Circ. No. 407 (U.S. GPO, Washington, D.C., 1952), Vol. 3.